Development and characterization of a laminar aerosol flow tube

Cite as: Rev. Sci. Instrum. **77**, 033102 (2006); https://doi.org/10.1063/1.2175958
Submitted: 22 July 2005 . Accepted: 22 January 2006 . Published Online: 10 March 2006

Alexei F. Khalizov, Michael E. Earle, Wayde J. W. Johnson, Gordon D. Stubley, and James J. Sloan

Development and characterization of a laminar aerosol flow tube

Alexei F. Khalizov and Michael E. Earle
Department of Chemistry, University of Waterloo, Waterloo, Ontario N2L 3G1, Canada

Wayde J. W. Johnson
Department of Chemistry, University of Waterloo, Waterloo, Ontario N2L 3G1, Canada
and Department of Mechanical Engineering, University of Waterloo, Waterloo, Ontario N2L 3G1, Canada

Gordon D. Stubley
Department of Mechanical Engineering, University of Waterloo, Waterloo, Ontario N2L 3G1, Canada

James J. Sloan
Department of Chemistry, University of Waterloo, Waterloo, Ontario N2L 3G1, Canada

(Received 22 July 2005; accepted 22 January 2006; published online 10 March 2006)

We have developed a new laminar aerosol flow tube (AFT) to study transformations such as ice nucleation, deliquescence, and efflorescence in model atmospheric aerosols. The apparatus consists of four sections which can be independently cooled to reproduce temperature profiles relevant to the troposphere and stratosphere. An automatic control system maintains the average axial temperature along each section between 100 and 300 K, within ±0.1 K. Changes in aerosol composition, phase, and size distribution are monitored at the tube exit using infrared spectroscopy (AFT-IR). We used computational fluid dynamics simulations to investigate flow velocity and temperature distributions within the flow tube. Based on these computations, the final design was formulated to eliminate turbulent mixing zones and buoyancy-driven convection cells. The latter can occur even under conditions where the Reynolds number indicates laminar flow. In either case, recirculation causes aerosol residence times and temperature histories to be poorly defined, leading to erroneous interpretation of experimental measurements. The resulting AFT design used copper fins to reduce temperature gradients and axial mixing of aerosol and carrier gas flows in the inlet section to reduce turbulence. The performance of the new AFT is significantly better than for previous designs. [DOI: 10.1063/1.2175958]

I. INTRODUCTION

Aerosols play an extremely important role in the chemistry and physics of the atmosphere. From catalysis of ozone depletion in the stratosphere to reduction of visibility during smog events in cities, aerosols are ubiquitous and active in atmospheric processes. Possibly their greatest importance to current atmospheric science is their role in climate change.[1] By influencing solar and terrestrial radiative transfer, they have a large, but very poorly understood, effect on the temperature of the troposphere. Their physical and chemical transformations are very important to the formation, growth, and phase changes of clouds, and as a result, it is very important to know the conditions under which these transformations occur.

Laminar aerosol flow tubes (AFTs) have been used widely to study the transformations and physical properties of aerosols under conditions typical of the troposphere and stratosphere since their introduction for this purpose more than a decade ago.[2] An aerosol, usually generated by atomization of liquid or by homogeneous or heterogeneous condensation of vapor, is introduced to the AFT in a carrier gas flow. After conditioning at a certain temperature and relative humidity, the aerosol passes to a region where these conditions are changed to initiate the process of interest, such as deliquescence, efflorescence, or freezing. The aerosol then passes to the detection section, where changes in its physical properties and size distribution are observed using infrared spectroscopy (AFT-IR). Using this approach, a wide range of chemical and physical processes have been studied, notably the transformations of aqueous electrolyte solutions and crystalline particles.[3]

Benefiting from more than a decade of experience with AFT-IR in our laboratory,[2,4,5] we have constructed a new vertical flow tube that represents a significantly improved version of the design that we first built in 1990. The new apparatus, which has fine temperature and flow control, in combination with a recently developed aerosol measurement procedure based on IR extinction measurements,[6] provides accurate, direct information about the size, physical state, and composition of aerosol particles.

During experiments on the ice nucleation rate in pure water aerosol using the first version of the new AFT apparatus, the measurements suggested that there were transient disturbances or turbulence in the flow, even though the Reynolds numbers were well within the laminar regime. Thermocouples placed at fixed locations in the gas flow showed unexpected temperature oscillations. Also, while observing water and/or ice aerosols at a variety of temperatures, both the amplitude of the IR signal (real time, single channel) and

the derived size distributions of the aerosols varied somewhat, even though the experimental conditions were held constant.

To reveal the source of this unexpected behavior, we used computational fluid dynamics (CFD) simulations to explore the temperature and flow regimes for different elements of our flow tube. These provided us with spatial velocity and temperature distributions in the gas flow that are either difficult or impossible to measure directly. Using this information, we modified our flow tube design in a way that significantly improved its performance. In addition, these CFD results assisted with the interpretation of our experimental measurements by providing information about particle residence times and temperature histories.

II. AFT DESIGN AND EXPERIMENTAL SETUP

The new AFT design is similar to previous versions[4,5] in the flow control system, means of aerosol generation, and optical configuration. The cooling system and temperature control, however, have been improved dramatically and the internal volume of the flow tube has been divided into four separate flow sections by inserting two flat copper strips (fins) at 90° along the tube axis. Some of these changes have been described briefly elsewhere.[7,8] The following section provides a comprehensive account of all components of the new AFT design.

A. Cryogenic aerosol flow tube apparatus

The new cryogenic aerosol flow tube apparatus is shown in Fig. 1. The flow tube is composed of four sections of copper pipe (37.5 cm long, 8.9 cm inside diameter (i.d.), and 0.6 cm wall thickness) joined by thin-walled stainless steel bellows (7.0 cm long, 8.9 cm i.d.), which ensure the thermal isolation of each section. In this way, temperature differences of about 100 K can be achieved between adjacent sections. Each copper section is connected to a bellows using stainless steel mating flanges, sealed with spring-loaded PTFE/Teflon® coated Wills Rings O® (American Variseal Corp.). These seals maintain their integrity under cryogenic conditions; the elasticity of the metal spring compensates for thermal variations in the hardware.

The flow tube and bellows comprise the inner assembly, which is enclosed within a vacuum jacket composed of 21.9 cm diam stainless steel pipe. The jacket is evacuated by a mechanical pump to approximately 0.1 mbar, preventing conductive heat transfer between the flow tube and the environment. Additionally, the inner assembly is wrapped with a few layers of aluminized Mylar® film to reduce radiative heat transfer from the vacuum jacket to the flow tube.

The vacuum jacket is divided into four 45.7 cm sections, each enclosing one copper flow section and bellows. Adjacent jacket sections are joined by stainless steel mating flanges and sealed with Buna O rings. Annular nylon supports located at the bottom of each section hold the inner assembly in the jacket center.

Each jacket section is equipped with two 15.2 cm diam stainless steel access ports (front and side) offset by 90°. The ports are capped with stainless steel end plates and sealed

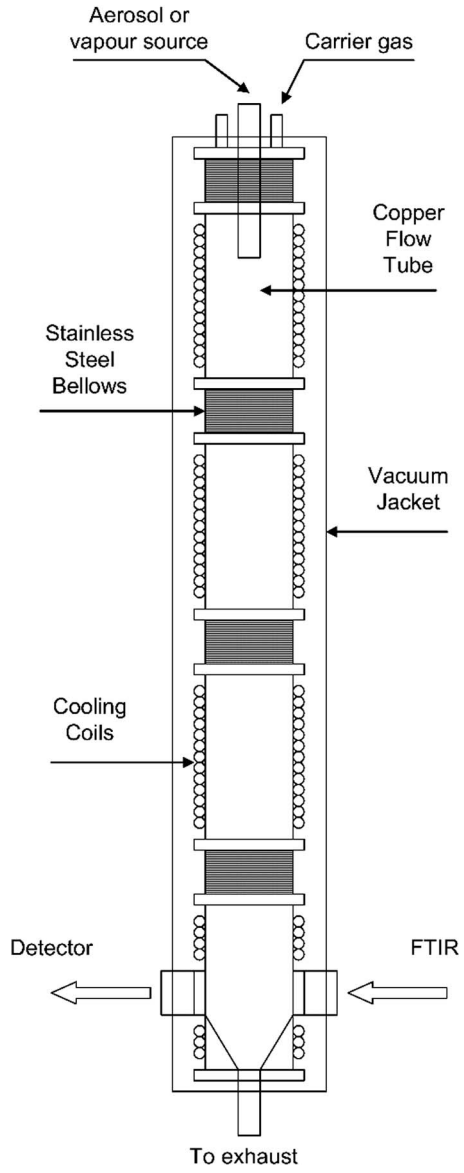

FIG. 1. Flow tube apparatus. An inner assembly comprised of four copper sections separated by stainless steel bellows is enclosed within an evacuated stainless steel jacket. Each section is equipped with copper cooling coils. The gas and aerosol enter the inner assembly at the top and exit at the bottom. The IR probe beam passes across the aerosol flow through optical ports in the bottom section.

with Buna O rings. Each end plate is fitted with an eight-pin feedthrough for four thermocouples and two feedthroughs for cooling lines to enter and exit the inner assembly. Each cooling line feedthrough is composed of concentric 0.6 and 1.3 cm diam stainless steel tubes, which are fillet-welded to minimize thermal contact. The weld was placed 6.4 cm from the base of the flange to the flow tube exterior to ensure that heat transferred to the outer pipe will dissipate before reaching the flange edge. This design prevents the flange and the corresponding O ring from freezing and compromising the vacuum integrity when cooling gas flows through the inner pipe.

The side access port on the top jacket section is equipped with a 1.9 cm i.d. Ultra-Torr adaptor (Swagelok Co.) through which a tube is passed to the top section of the flow tube interior. This tube can be employed as a side inlet. The end

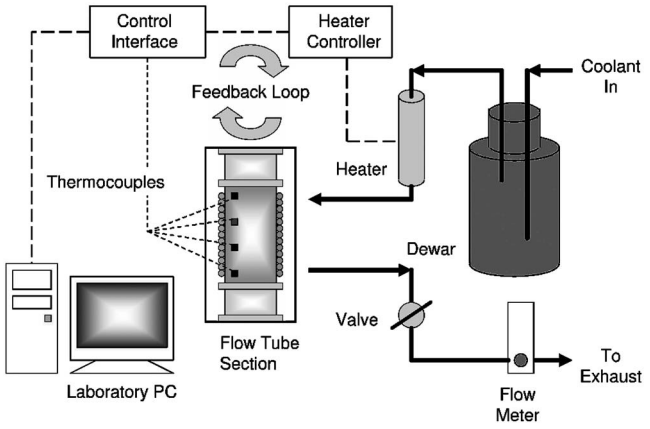

FIG. 2. Temperature control system. Pressurized liquid nitrogen is passed to a stainless steel Dewar where it partially evaporates or is converted into spray. The liquid and/or gaseous nitrogen then flows to the cooling coils. Individual section temperatures are monitored using thermocouples and adjusted using in-line heaters, all through a computer interface and LABVIEW code.

plate on the second topmost jacket section connects the jacket interior to a vacuum line through a flexible metal hose.

B. Cooling system and temperature control

A schematic drawing of the flow tube temperature control system is shown in Fig. 2. The cooling system comprises an external network of Styrofoam-insulated 1.3 cm o.d. copper lines coupled to 0.6 cm o.d. copper cooling coils, which are secured to the outer wall of each section of the flow tube with thermally conductive epoxy (T7109, Epoxy Technology, Inc.). A mixture of liquid and gaseous nitrogen is supplied from a tank at 7 bar through an insulated line to a 30 L stainless steel Dewar. A cryogenic solenoid valve (8222G2LT/AC, Asco Valve Inc.) controls the flow of nitrogen coolant into the Dewar. The relative proportion of liquid to gaseous nitrogen varies with the consumption rate; the greater the refrigerant flow, the more liquid nitrogen passes into the Dewar. When the liquid nitrogen reaches the level of the delivery tube in the Dewar, spray consisting of small droplets of liquid nitrogen is generated, significantly increasing the cooling efficiency. At typical flow rates employed to maintain flow tube temperatures in the vicinity of 235 K, the nitrogen flow is primarily gaseous.

Immediately following the Dewar reservoir, the coolant flow is split into four separate lines—one for each section of the flow tube. These flows are controlled manually using four Swagelok bellows valves (SS-BNS4) and four floating-ball flow meters (model 5671003-01-001, Controls Corporation of America) located after the flow tube. The 1.3 cm diam lines carrying the coolant to the apparatus are then connected to the feedthroughs described above. Inside the vacuum jacket, the coolant is delivered to the cooling coils via a 30.5 cm length of thin-walled, convoluted stainless steel tubing (Swagelok Co.).

Each copper section is wrapped with two concentric cooling coils of 0.6 cm diam copper tubing. The coolant is introduced at the top of the outer coil, flows downward, and from the bottom it is transferred to the top of the inner coil, through which it flows downward again. Tests of different flow configurations indicate that this parallel flow provides the most efficient and uniform cooling relative to alternative pathways. After circulating through both coils, the nitrogen coolant exits at the bottom of the inner coil and leaves the apparatus via a second 30.5 cm length of convoluted stainless steel tubing connected to the second feedthrough. At the exit, it passes through the flow control valves described previously.

This cryogenic AFT system has the ability to maintain temperatures ranging from 100 to 300 K. The independent cooling of individual sections allows a wide variety of axial temperature profiles to be employed. Fine temperature control is achieved through the use of 400 W in-line electrical heaters (AHP-5051, Omegalux Co.) located along the inlet cooling line of each section. These heaters have been modified for operation under cryogenic conditions by replacing the epoxy seal through which the electrical leads exit the heater with a two-conductor feedthrough (CeramTec North America, Corp.) in a 1.3 cm Swagelok fitting. Voltage applied to the heaters by an electrical controller warms the inlet nitrogen gas. To prevent overheating, thermocouples attached to the body of each heater are monitored by a controller, and should the temperature exceeds the set threshold (typically 323 K), the heater voltage is removed.

The temperatures of the AFT sections are monitored using 16 type T (copper/constantan) thermocouples (Special Limits of Error Wire, Omega Engineering, Inc.)—four per section—attached to the outer wall of the copper flow tube. For each section, the first thermocouple is 5.1 cm from the top and the remaining three are located at 8.9 cm intervals below it. Each is secured to the wall with aluminum adhesive tape.

The thermocouples and heaters are integrated via a FieldPoint modular distributed input/output (I/O) interface (National Instruments FP-1601, FB-TC-120, and FP-TB-10) and operated by LABVIEW code. This code allows the temperature of each section to be independently monitored, set, and controlled. Following initial equilibration, the average temperature of a section wall typically remains within ±0.1 K of the set point. Direct measurements show that axial temperature deviations along a section are within ±0.5 K.

A set of cross-shaped copper fins (Fig. 3) is placed in each section of the flow tube to augment radial heat transfer (see Sec. IV B). The fin mounts provide firm and secure contact with the flow tube wall. The fins in the two middle sections extend 5.1 cm into the bellows above—without touching the bellows wall—to provide smoother temperature transitions between the sections.

C. Aerosol generation and flow control

The total nitrogen flow through the AFT is controlled by a mass flow controller (810 C Mass-Trak, Sierra Instruments, Inc.), which is operated via the FieldPoint modular distributed I/O interface by LABVIEW code. After passing through the mass flow meter, the nitrogen flow is split into separate streams for the bulk carrier gas, humidified carrier gas, aerosol source, and window purge flows. These flows are controlled independently using a series of floating-ball flow

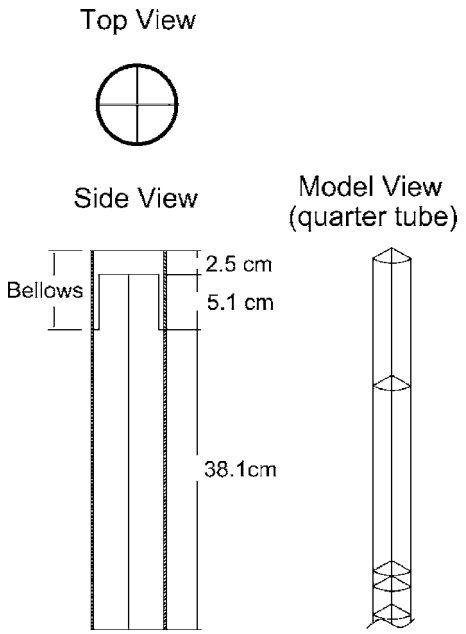

FIG. 3. Top and lateral views of a flow tube section with copper fins inserted and part of the model used to simulate the flow.

meters (Advanced Specialty Gas Equipment FM4333 and FM4334). The aerosol or aerosol precursor (vapor or vapor with condensation nuclei) is introduced to the apparatus in a nitrogen flow [0.5–3.0 SLPM (standard liters per minute)] and then mixed with additional nitrogen carrier gas (3–15 SLPM) in the top section of the flow tube to adjust aerosol size and number density, as well as the relative humidity.

The liquid aerosols to be studied can be generated inside the flow tube, through homogeneous or heterogeneous condensation of supersaturated vapor, or can be generated externally. An ultrasonic nebulizer (Ultra-Neb 99, DeVilbiss Co.) is used to produce particles in the 1–6 μm diameter range. Smaller particles (0.3–3 μm diameter) are generated using a constant output atomizer (TSI 3076, TSI Inc.). In both cases, the aerosol flow is introduced to the apparatus via a temperature controlled glass inlet approximately 50.8 cm long. The inlet comprises two concentric tubes: a 2.5 cm o.d. inner tube delivers the aerosol flow and a 3.8 cm o.d. outer tube encloses the inner tube and heating assembly. This assembly consists of three wire-wound silicon rubber heaters (Minco Products, Inc.) affixed to thin copper sheets, wrapped around the inner tube. Each heater is controlled independently using one of the three Powerstat® autotransformers. The copper fin assembly in the top section of the flow tube is modified to accommodate the glass inlet.

The glass inlet enters the top section of the flow tube through a 3.8 cm diam Quick Disconnect adaptor (MDC Vacuum) located in the center of the flow tube lid, which is a 17.1 cm diameter stainless steel plate sealed to the vacuum jacket with a spring-energized PTFE/Teflon® coated O ring. The lid is also equipped with four equally spaced 1.3 cm inlets, positioned on a 3.8 cm diam circle. These inlets are connected to the carrier gas manifold.

Below the lid, the carrier gas is precooled by passing around a 7.6 cm long cylindrical coil of 0.6 cm diam copper tubing connected to the outlet of the top section cooling line. In this way, the temperature of the precooling coil is automatically adjusted upon changes in the temperature of the top section.

D. Optical configuration

The bottom section of the flow tube is equipped with reentrant optical ports for spectroscopic observation. These ports are located 25.4 cm below the top of the section on opposite sides of the flow tube. A shortened set of copper fins is placed in the upper 22.9 cm of the section to avoid obscuring the optical path. The ports comprise 6.4 cm i.d. stainless steel bellows, sealed on the outside with KRS-5 windows. A slow flow of nitrogen (0.05 SLPM) is directed towards the inner surface of each window from four points arranged around the window perimeter to prevent vapor condensation and aerosol deposition. A collimated IR beam modulated by a Michelson interferometer (Bruker Tensor 37) intersects a cylindrical section of the aerosol flow between the observation windows and is focused by an off-axis parabolic mirror onto a mercury cadmium telluride (MCT) detector (FTIR-22-1.0, Infrared Associates, Inc.) on the opposite side of the flow tube.

Spectra are recorded and processed using Bruker OPUS software. Each spectrum is typically an average of 80 scans collected in the range from 450–6000 cm^{-1}, at 2 cm^{-1} resolution and 40 kHz metrology frequency. To obtain pure aerosol spectra, water vapor spectra recorded at the same temperatures are routinely subtracted from the measured extinction spectra.

III. COMPUTATIONAL FLUID DYNAMICS MODEL

To guide the design of the AFT for optimal flow conditions, a CFD model of the important parts of the flow tube was developed. This model allowed easy examination of experimental variables (tube geometry, flow rate, section temperatures, etc.) and analysis of the corresponding flow field properties, such as velocity, temperature, and the presence of recirculation zones. The CFD model was created using ANSYS WORKBENCH software (ANSYS, Inc.) for geometry and mesh generation. The cell-centered control volume method with face-based assembly was used for matrix construction. The matrix was solved using an iterative method and multigrid algorithms. CFX software (ANSYS, Inc.) was used for setting the boundary conditions and fluid properties and finding the numerical solutions for the flow fields. A second order upwind differencing scheme was used with gradient reconstruction for predicting the flow properties through the control volume faces.

Two regions of the apparatus constructed in our laboratory were modeled using CFD: the straight region of the flow tube and the inlet region. The geometry of each of the modeled flow tube regions is shown in Figs. 3 and 4, respectively. Note that in Fig. 3, only one quarter of the tube was modeled due to the fourfold symmetry of the fin structure. The simulation considered the gas flow in the straight region to be buoyant, laminar, and incompressible. The Reynolds number was small—approximately 100 based on the hydraulic

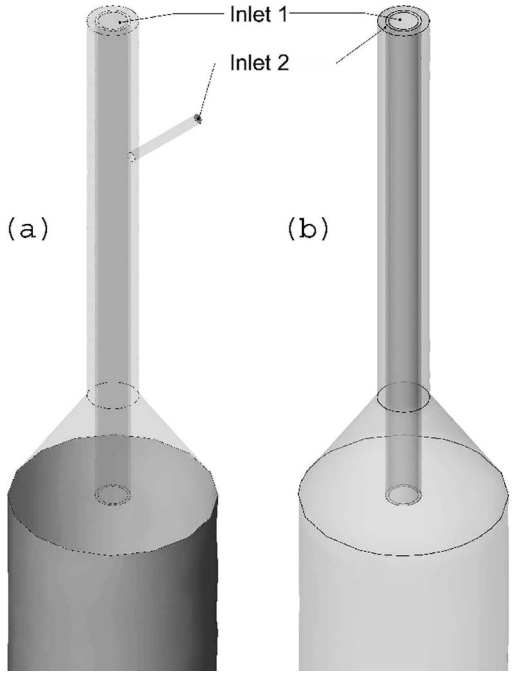

FIG. 4. The geometry for the model simulating the inlet region for (a) the side inlet and (b) the annular inlet. Both inlet regions interface directly with the top of the straight section of the flow tube (shown in Fig. 1).

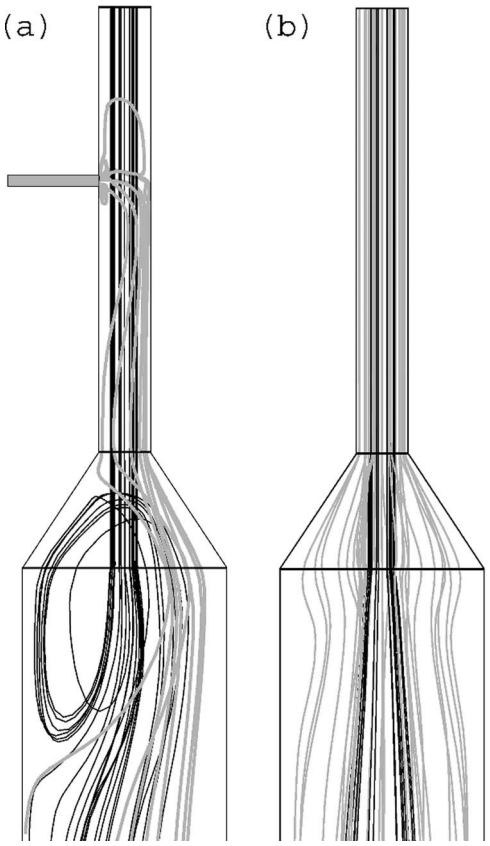

FIG. 5. Streamlines showing the flow pattern near the inlet and expansion areas for (a) the side inlet design and (b) the improved annular inlet design. In each case, the aerosol flow was 3 SLPM and the carrier flow was 1 SLPM.

diameter—whereas the transition to turbulent flow in round pipes occurs at a Reynolds number around 2300, making the occurrence of turbulence highly unlikely. It is still possible, however, that unsteady, laminar recirculation zones may develop. The velocity condition applied to the model walls was no slip (zero velocity). Wall temperature profiles used in the CFD model were constructed by interpolation of readouts from the 16 thermocouples on the flow tube wall (see Sec. II B); additional temperature measurements were made at several points on the interior of the flow tube wall and on the bellows. The fins were modeled with a constant temperature equal to that of the walls; this condition was verified by direct measurement and analytical calculation. The inlet boundary condition was of uniform velocity and temperature, and at the outlet a nominal average static pressure was set. The inlet was extended in the CFD model to allow for flow development, so the uniform velocity profile had a negligible effect on the flow in the AFT interior, despite the possibility that flow disturbances might result from mixing gases of different velocities, one of which had passed over cooling coils. The fluid properties were constant and were for those of air at a representative flow tube temperature (based on the inlet temperature and boundary condition temperature). The temperature variations within the flow tube were small enough that changes in fluid properties throughout the flow domain were negligible.

The inlet region was modeled using the same approach, with the exception of turbulence. Due to the higher velocities in the inlet region, the Reynolds number exceeded 2300, and therefore a turbulence model was applied. The $k-\varepsilon$ turbulence model was used, with a standard wall function. Wall functions are commonly used in turbulent simulations to estimate the boundary layer physics; otherwise, a very fine mesh would be required at the wall, because turbulent boundary layers are very thin (wall models are not required in laminar flow simulations, such as that of the straight section of the flow tube). All numerical solutions were obtained on discrete meshes with tetrahedral and prism elements. For each flow model a systematic mesh refinement study was performed; the results presented for each case were obtained on meshes with mesh discretization errors below 0.1%. The discrete nonlinear algebraic equation set was iteratively solved until the maximum normalized residual (equation imbalance) was below 1×10^{-4}. The CFD model results were compared with experimental data for validation; this approach has been used previously in similar studies.[9]

IV. FLOW TUBE PERFORMANCE

A. Inlet design

The aerosols are either created or their sizes are adjusted, in the inlet region, so it is important to control the conditions here very carefully. The initial design of the top section used a straight axial inlet to introduce aerosol and carrier gas (3 SLPM) and a side inlet to introduce additional carrier gas (1 SLPM), as shown in Fig. 4(a). This configuration caused recirculation of the gas near the flow tube entrance as shown in Fig. 5(a). Recirculation in the inlet region leads to significant particle growth in two ways: first, particles produced by homogeneous or heterogeneous nucleation of supersaturated vapor can experience additional growth if they return to the

region of the tube in which they were formed and second, recirculation leads to collisions between aerosol particles, causing agglomeration. The net result is that the particles become bigger, and their number density decreases in an uncontrollable manner. To address this problem, we designed a coaxial inlet in which the aerosol and carrier gas are both introduced along the axis of the flow tube [Fig. 4(b)]. The result can be seen in Fig. 5(b), which shows that for the same experimental conditions (3 SLPM aerosol flow, 1 SLPM carrier flow), recirculation can be eliminated, while mixing is still efficient. Mixing is enhanced when the velocity through the central tube is higher than that through the external tube. This causes an entrainment effect, which draws the external flow inward, thereby reducing the mixing length. If the velocity mismatch is too large, however, the increased entrainment rate can lead to recirculation within the flow tube. The improvements evident from the flow streamlines in Fig. 5(b) relative to those in Fig. 5(a) are due solely to changes in the inlet geometry; in both cases, the same flow rates and inlet conditions (uniform velocities with a turbulent intensity of 5% and a turbulent viscosity of ten times the molecular viscosity) were used.

It is imperative that recirculation in the inlet region be minimal, as this region interfaces directly with the top of the straight section of the flow tube (Fig. 1). The configuration that was ultimately implemented is described in Sec. II C. This design allows the aerosol or humidified nitrogen flow to be delivered directly into a stream of prechilled carrier gas. The humid central inlet flow is kept at a temperature above 273 K to avoid blocking the exit orifice with ice.

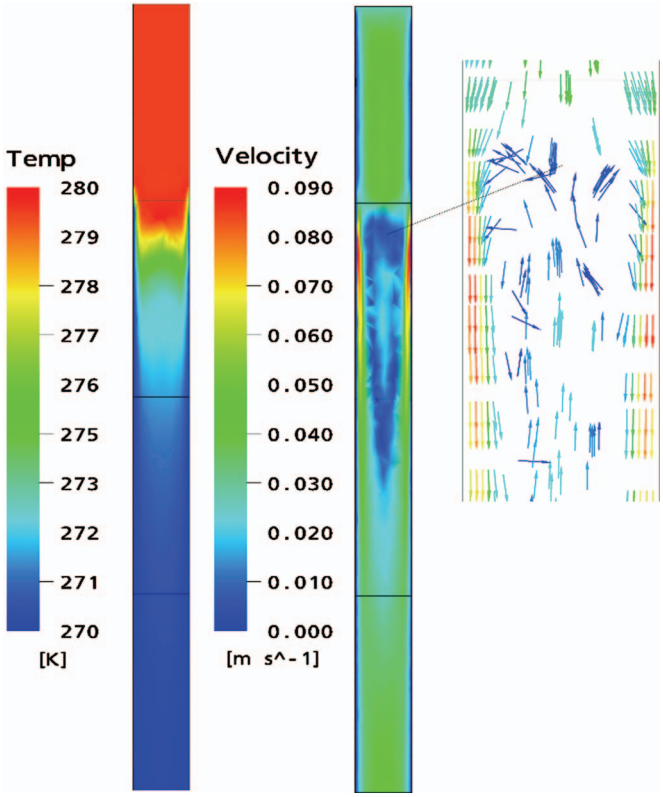

FIG. 6. (Color) Temperature and velocity contours within the flow tube without fins for a typical cooling scenario (flow velocity of 3 cm s^{-1}, inlet temperature of 280 K, wall temperature of 270 K, and flow tube diameter of 9.0 cm). The inset shows the recirculation present under these conditions.

B. Wall-to-gas heat transfer

We modeled a typical experiment in which gas travels with a velocity of 3 cm s^{-1} down a straight, vertical tube with an inner diameter of 9.0 cm, passing from a warm section to a cold section. For the range of temperature differences over which inertial and buoyancy forces are comparable (mixed convection), the effects of buoyancy can be significant. In this particular case, the top section of the flow tube was held at 280 K while the lower three sections were held at 270 K. As shown in Fig. 6, the gas near the wall cools faster than that in the center of the tube, because in a laminar flow (Reynolds numbers in the range from about 50 to 500), molecular mixing is slow and the rate of heat conduction by the gas is limited. Since the colder gas near the wall is more dense, it travels downward more quickly relative to the gas in the center. If the downward mass flow rate near the wall becomes high enough, mass conservation requires that the flow in the center of the tube moves upward creating a recirculation zone. This recirculation facilitates heat transfer between the gas and tube wall but causes the residence time for the aerosol particles to be undetermined, as they can cross the boundary between the warm and cold zones many times. This may lead to complex aerosol transformations, such as the freezing of a few droplets at lower temperature, followed by their growth at the expense of the remaining liquid droplets.[10] when these nascent ice particles are transported to the warmer zone. Liquid particles may also grow due to collision-induced coagulation, which is greatly promoted by this recirculation.

As will be further discussed in the following section, convection-driven recirculation can be suppressed by using faster flow velocities and smaller tube diameters. Implementation of the former requires a proportional increase in flow tube length to maintain particle residence times, while the latter reduces the observation path length, lowering the detection sensitivity. To overcome these disadvantages, we inserted copper fins into the flow tube, as shown in Fig. 3. These reduce the effective diameter of the flow channels, permitting a reasonably short apparatus length without reducing the observation path length. The fins also help to straighten the flow, and they propagate the wall temperature radially in approximately 40% of the time required in their absence.

In the middle two sections of the flow tube, the fins extend upward into the bellows above without touching the bellows walls. These extensions begin to change the temperature of the gas while it is still in the bellows. For the case discussed in the previous section, these extensions cool the flow close to the central axis, thereby accelerating the core, which balances the effect of the cold walls and prevents the formation of the recirculation zones shown in Fig. 6.

The CFD analysis of the improved heat transfer that results from this configuration is shown in Fig. 7. While a very small residual velocity change remains near the wall, this is not significant by comparison with the total flow. The wall temperature boundary conditions in this case were based on

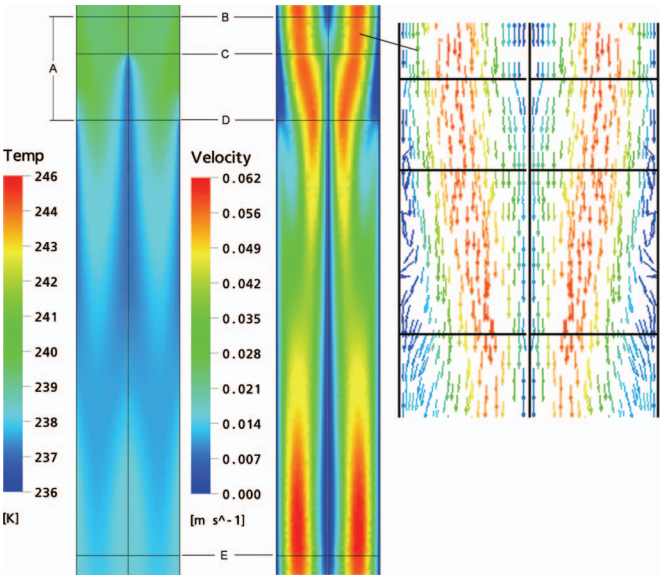

FIG. 7. (Color) Temperature and velocity contours within the flow tube after the addition of copper fins (flow velocity of 3 cm s^{-1}, inlet temperature of 246 K, wall temperature of 236 K, and flow tube diameter of 9.0 cm). A—bellows region, separates sections of the flow tube; B—end of the second section; C—fins begin; D—third section begins; E—third section and fins end.

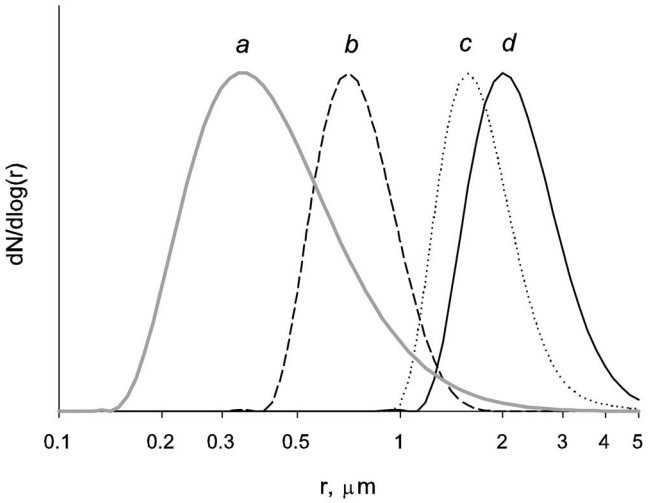

FIG. 8. Effect of flow tube diameter and flow velocity on the evolution of water aerosol produced by TSI 3076 atomizer. Particle number size distributions are shown for different tube diameter (cm)/velocity (cm s^{-1})/residence time (s)/buoyancy parameter: (a) 1.3/40/0.1/0.003, (b) 3.8/4.4/110/0.79, (c) 4.5/2.7/70/2.47, and (d) 8.9/0.8/220/56. The size distributions have been scaled for display purposes.

experimental measurements of the actual wall temperature. The wall temperature is not axially uniform in each section because of the heat transfer from the coolant flow to the cooling coils. This warms the coolant as it passes through the coils, and as a result, the wall temperature rises slightly near the end of the section. This slight temperature increase accounts for the warming of the flow observed in Fig. 7.

It is evident from Fig. 7 that the coldest temperatures in the flow tube interior are found at the tube wall and fins. These cold surfaces can thus serve as sinks where vapor can condense and/or freeze, depending on the aerosol properties and experimental conditions. The inclusion of fins significantly increases the available surface area for this condensation and/or freezing to occur. The diffusive loss to the fins, however, can be accounted for quite easily, and the effects of vapor loss are thus a small price to pay for the benefits of minimizing convection cells.

C. Effect of convection on aerosol size distributions

Even when all flow tube sections have nearly the same temperature, convection currents arising from small residual temperature gradients may interfere with laminar flow at the low bulk flow velocities typically used in AFTs. The state of such mixed convective flow, which was introduced in the previous section, can be analyzed using the buoyancy parameter:[11]

$$\frac{\mathrm{Gr}}{\mathrm{Re}^2} = \frac{[g\beta L^3 \Delta T/\nu^2]}{[\rho \bar{u} L/\mu]^2}, \tag{1}$$

where Gr is the Grashof number, Re is the Reynolds number, g is gravity, β is the volumetric thermal expansion coefficient, L is the characteristic length of the geometry (in this case, the hydraulic diameter of the flow tube), ΔT is the temperature difference between the tube wall and flow, ν is kinematic viscosity, ρ is density, $\bar{u}$ is average velocity, and μ is molecular viscosity. The buoyancy parameter $\mathrm{Gr}/\mathrm{Re}^2$, is a dimensionless value that compares the strength of buoyancy forces with that of inertial forces. When $\mathrm{Gr}/\mathrm{Re}^2$ is greater than unity, the flow is dominated by buoyant forces. For instance, in the absence of the fins in our flow tube, a temperature difference of 1 K yields $\mathrm{Gr}/\mathrm{Re}^2 \sim 3.8$ for a flow velocity of 3 cm s^{-1}. The buoyancy parameter is proportional to the tube diameter and the temperature difference and inversely proportional to the square of the average velocity, so buoyant recirculation in the flow can be controlled by adjusting these three variables. In the case of our apparatus, the addition of the fins reduced the hydraulic diameter of the tube by more than a factor of 2, and this, combined with an increase in the flow speed, suppressed the formation of buoyant recirculation cells. Although the most effective way to reduce the buoyancy parameter is to increase the average flow velocity, one must ensure that the Reynolds number remains below the critical value for laminar flow.

We confirmed the simple estimations presented above in a series of experiments on pure water aerosol in flow tubes having different diameters and different flow velocities. During these measurements, the flow tubes were held at room temperature but were not thermally insulated, so maximum temperature variations of about ±1 K occurred. Water aerosol was produced using a constant output atomizer; humidified nitrogen was mixed coaxially with the aerosol flow to increase the flow velocity. Figure 8 illustrates the effect of tube diameter and flow velocity on the aerosol size distributions, which were obtained from infrared extinction spectra using the characterization procedure described previously.[6] The distributions were obtained from single experimental runs obtained when the flow tubes were operated in a steady state regime; the distributions are highly reproducible. The largest particles [Fig. 8(d)] were observed in a flow tube of large diameter (8.9 cm) at low velocity (0.8 cm s^{-1}). When

the cross-shaped fins described earlier (see Fig. 3) were installed to decrease the effective diameter to 3.9 cm and the flow velocity was increased to 2.7 cm s^{-1}, smaller particles were observed [Fig. 8(c)]. The substantially smaller size distribution shown in Fig. 8(b) was achieved by increasing the flow velocity to 4.4 cm s^{-1}, and performing the experiment in a 3.8 cm diam tube.

For comparison, Fig. 8(a) also shows the size distribution for a water aerosol recorded in a small cell connected directly to the atomizer exit. These particles are significantly smaller than those observed in 8(b)–8(d), where the aerosol had been transported a distance of 1–5 m in the flow tube before detection. Aerosol produced by the atomizer is usually cooler than the ambient environment, as a substantial amount of water evaporates in the atomizer to saturate the initially dry carrier gas. After exiting the atomizer, the aerosol warms up and partially evaporates. In addition, submicron particles produced by the atomizer can grow due to recondensation caused by the Kelvin effect, as well as collision-induced coagulation. At this point, the particle distribution quickly stabilizes and any further condensation is minimal. Thus, we attribute the increase in particle size observed when the aerosol had been transported further from the atomizer (increased residence time) to be due primarily to collision-induced coagulation of droplets. This coagulation is greatly exacerbated by the existence of convection-driven recirculation cells. The trends in the size distributions presented in Fig. 8 are consistent with Eq. (1), which shows that decreasing the tube radius and increasing the flow velocity lowers the Gr/Re^2 ratio, thereby lowering the contribution of buoyancy forces. Assuming that the maximum temperature difference between the tube wall and flow is 1 K (due to the natural temperature variations noted above), the buoyancy parameter values corresponding to the scenarios for Figs. 8(a)–8(d) are 0.003, 0.79, 2.47, and 56, respectively.

D. Axial and radial temperature profiles

It is widely assumed that the axial flow temperature changes sharply when the flow passes from "warm" to "cold" regions of an AFT. This is not correct. Figure 9 shows temperature profiles in our AFT (with fins inserted) for a temperature drop of 4.55 K between the second and third sections (sections B and C). It is apparent that, even for this relatively small temperature gradient, cooling is not instantaneous in a laminar flow. Instead, the measured flow temperature in the geometric center of the quarter tube cross section (black triangles) lags behind the wall temperature (gray circles) by up to 3 K for approximately the first 25% of the distance into the cooled section. Prior to the inclusion of fins, the centerline temperature had lagged behind the wall temperature for longer distances and, in some cases, for the length of the entire sections. Since aerosol transformations (e.g., ice nucleation)[12] are highly temperature dependent, detailed knowledge of the axial temperature evolution is crucial when measuring or modeling the kinetics of these processes. The axial temperature profile is readily measured in the center of the flow, but this is not adequate for modeling aerosol transformations, because the particles are spread out over the entire cross section and the radial temperature distribution is

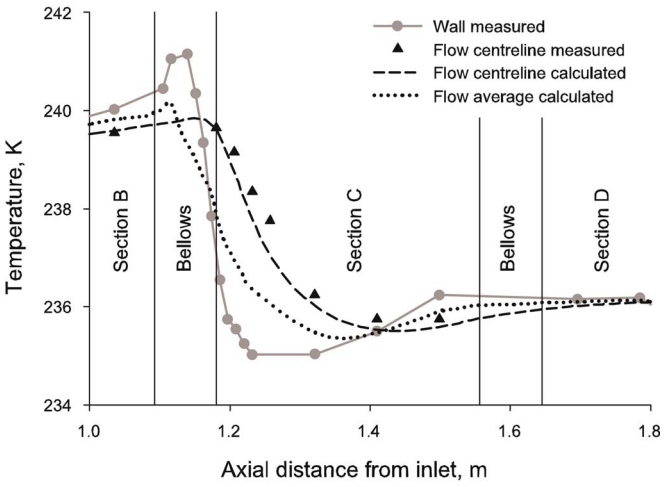

FIG. 9. Axial temperature distribution within the flow tube after the addition of copper fins; flow velocity of 3 cm s^{-1}; average wall temperature transition from 240 (section B) to 235.5 K (sections C and D); flow tube diameter of 9.0 cm (see Fig. 7 for tube geometry). Note that tube sections are labeled A–D, top to bottom.

generally not constant with axial distance (see Fig. 7). In practice, it is difficult to measure the cross-sectional temperature distribution in the gas, but using CFD, it can be modeled very accurately if the tube geometry and wall temperatures are known. This is illustrated by the dashed and dotted curves in Fig. 9. The dashed curve shows the CFD calculation of the centerline temperature profile, which differs from the measurement by less than 0.5 K, illustrating the accuracy of the CFD calculation. The dotted curve shows the mass-weighted average temperature, which differs from the centerline and wall temperatures by up to 2 K at points where the temperature is changing rapidly. Thus, it is important to have a cross-sectional temperature distribution, or at least a cross-sectional average temperature, that is more representative than the centerline temperature of the conditions to which aerosol is subjected as it travels along the flow tube. The excellent agreement between measured and calculated centerline gas temperatures shown in Fig. 9 is an example of the capability of CFD to represent thermal transfer accurately. Similar results were obtained from runs in which the top section was held at 240 K, and the lower three sections were maintained at constant temperature between 238.6 and 234 K. We therefore believe that CFD can provide accurate mass-averaged temperature values for use in the modeling of aerosol transformations in AFTs.

ACKNOWLEDGMENTS

The authors are grateful for the financial support of the Natural Sciences and Engineering Research Council of Canada and the Canadian Foundation for Climate and Atmospheric Studies. The authors wish to thank the University of Waterloo Science Technical Services for their contribution to the design and construction of the experimental apparatus.

[1] J. T. Houghton, Y. Ding, D. J. Griggs, M. Noguer, P. J. van der Linden, X. Dai, K. Maskell, and C. A. Johnson, *Climate Change 2001: The Scientific Basis: Contribution of Working Group I to the Third Assessment Report of the Intergovernmental Panel on Climate Change* (Cambridge University

Press, New York, 2001).
[2] R. Callaghan, I. J. Lim, D. E. Murdock, J. J. Sloan, and D. J. Donaldson, Geophys. Res. Lett. **21**, 373 (1994).
[3] D. J. Cziczo and J. P. D. Abbatt, J. Geophys. Res., [Atmos.] **104**, 13781 (1999).
[4] A. K. Bertram and J. J. Sloan, J. Geophys. Res., [Atmos.] **103**, 3553 (1998).
[5] D. B. Dickens and J. J. Sloan, J. Phys. Chem. A **106**, 10543 (2002).
[6] A. Y. Zasetsky, A. F. Khalizov, and J. J. Sloan, Appl. Opt. **43**, 5503 (2004).
[7] A. Y. Zasetsky, A. F. Khalizov, and J. J. Sloan, J. Chem. Phys. **121**, 6941 (2004).
[8] A. Y. Zasetsky, A. F. Khalizov, M. E. Earle, and J. J. Sloan, J. Phys. Chem. A **109**, 2760 (2005).
[9] A. N. Kockevsky, e-print physics/0509192.
[10] H. M. Hung and S. T. Martin, Appl. Spectrosc. **56**, 1067 (2002).
[11] F. P. Incropera and D. P. DeWitt, *Fundamentals of Heat and Mass Transfer*, 5th ed. (Wiley, New York, 2002).
[12] H. R. Pruppacher and J. D. Klett, *Microphysics of Clouds and Precipitation* (Kluwer Academic, Boston, 1998).